Journal of King Saud University – Science 34 (2022) 102262

HOSTED BY

Contents lists available at ScienceDirect

Journal of King Saud University – Science

journal homepage: www.sciencedirect.com

Original article

Mixed perovskite ($MAPbI_{3-x}Cl_x$) solar cells using light-emitting conjugated polymer DMP end-capped MDMO-PPV as a hole transport material

Saradh Prasad [a,b], Mamduh J. Aljaafreh [c], Abeer Alshammari [a], Mona A.S. Almutairi [a], Jagannathan Madhavan [d], Mohamad S. AlSalhi [a,b,*]

[a] Department of Physics and Astronomy, College of Science, King Saud University, 11451 Riyadh, Saudi Arabia
[b] Research Chair on Laser Diagnosis of Cancers, Department of Physics and Astronomy, College of Science, King Saud University, 11451 Riyadh, Saudi Arabia
[c] Department of Physics, Imam Mohammad Ibn Saud Islamic University (IMISU), Saudi Arabia
[d] Solar Energy Lab, Department of Chemistry, Thiruvalluvar University, Vellore 632115, Tamil Nadu, India

ARTICLE INFO

Article history:
Received 18 May 2022
Revised 21 June 2022
Accepted 30 July 2022
Available online 4 August 2022

Keywords:
MAPbI3-xClx
MDMO-PPV
Solar cell
Perovskites
Conjugated polymers
Heterojunction
Li-TFSI

ABSTRACT

A series of solar cells (SCs) with methylammonium mixed halide perovskite active layers with a conjugated polymer (CP) poly[2-methoxy-5-(3,7-dimethyl-octyloxy)-1,4-phenylenevinylene] and end-capped with dimethylphenyl (MDMO-PPV) as a hole transport material (HTM) was fabricated under the same experimental settings, and the performance characteristics of the individual cells were compared. For comparison purposes, we fabricated a perovskite solar cell (PSC) with a lithium bis(trifluorome thanesulfonyl)imide (Li-TFSI)-doped sprio-OMeTAD layer (LiTSO), which showed a power conversion efficiency (PCE) of 7.68 %. The layered solar cell with a structure of TiO_2, perovskite and MDMO-PPV layers showed a PCE of 5.32 % and a fill factor of 0.478. The heterojunction solar cell (HJSC) made with a perovskite and MDMO-PPV mix showed a PCE of 5.68 %. The Field emission scanning electron microscope (FESEM) showed that in HJSC, the perovskite and CP were mixed well. However, they did not penetrate deeply into the TiO_2 mesoporous layer, which would hinder electron transportation and thus cause efficiency loss. The HJSC structure was tested using different thicknesses of mesoporous TiO_2 (m-TiO_2). At an optimal m-TiO2 thickness, the blend of perovskite and MDMO-PPV infused up to 350 nm, thus improving the PCE to 7.438 % and retaining 91 % performance even after 4 weeks of continuous operation. The perovskite/conjugated polymer blend also formed a small SC above the m-TiO_2 layer, showing complete penetration of the perovskite into the m-TiO_2 layer. Additionally, the formation of a pure perovskite layer on top of the TiO2/perovskite and MDMO-PPV covers neatly on top of the perovskite layer and serves as a protective layer as well as a hole transport layer. An additional layer of LiTSO on top of the HJSC further improved the PCE to 7.76 %. The use of a CP as the hole transport layer reduces the dependency on separate materials and improves the device's stability. It could also pave the way for an easy minimalistic method for integrated, flexible power electronics that contain solar cells (perovskite/conjugated polymer), organic light-emitting diodes, and supercapacitors made of graphene.

1. Introduction

In the previous decade, investigation pursuits on hybrid organic–inorganic lead halide-based perovskite solar cells have greatly increased, creating devices with power conversion efficiencies exceeding 23 %, which is pentafold as high as the first cells revealed in 2009 (Kojima et al., 2009; Yang and You, 2017). These devices utilize a lead halide perovskite as the primary light-absorbing layer with excellent optoelectronic characteristics, including a superior absorption coefficient, extended charge carrier diffusion length, small exciton binding energy, and bandgap

* Corresponding author.
E-mail addresses: srajendra@ksu.edu.sa (S. Prasad), maljaafreh@imam.edu.sa (M.J. Aljaafreh), Aalshammri@ksu.edu.sa (A. Alshammari), malsalhi@ksu.edu.sa (M.S. AlSalhi).
Peer review under responsibility of King Saud University.

Production and hosting by Elsevier

https://doi.org/10.1016/j.jksus.2022.102262
1018-3647/

tunable (Chen et al., 2015; Kim et al., 2012; Leijtens et al., 2014; Noh et al., 2013; Stranks et al., 2013; Wehrenfennig et al., 2014; Zheng et al., 2015). Using simple solution-based processing techniques, they are feasible and can be synthesized at a low cost. Methylammonium lead iodide ($CH_3NH_3PbI_3$ or MAPI) is the utmost often utilized active layer among the numerous perovskite materials available and is relatively easy to produce (Leguy et al., 2015; Tvingstedt et al., 2014). Researchers have been looking into mixed cations Formamidinium (FA), Cesium (Cs), and other halides, particularly Cl- and Br-based mixed perovskites, because of their sensitivity to degradation under environmental conditions, particularly that of temperature and humidity (Miyasaka, 2021; Tan et al., 2018). Studies have generally found smooth surfaces and high surface coverage in perovskite ($CH_3NH_3PbI_3$) films made from lead acetate-based precursors (Huang et al., 2016; Zhang et al., 2015). Through single-step spin coating process, the rapid elimination of methylammonium acetate (CH_3NH_3Ac) as a byproduct was achieved and it resulted in the creation of smooth, pinhole-free perovskite films with miniscule grain sizes. Rapid crystallization causes huge defects and high trap densities in the perovskite layer, which manifest as recombination centers and traps at the grain borders, lowering the photovoltaic characteristics of such solar harvester devices (Qing et al., 2015; Shao et al., 2014).

High-efficiency solar cells based on perovskites mostly employ a sophisticated environmental control comparable to that of semiconductor fabrication labs. Despite decades of advancement, we now know that not all countries can make their own semiconductor fabrication labs due to the many commercial and industrial prerequisites. There would be much less strain on productivity on a large scale if the strict environmental requirements were reduced. Furthermore, if we mitigate the defects and improve the stability of Perovskite SC, solar cells, even with PCE of 10–14 % and durability of 7–10 years, could become commercially viable and cheap solar cells and could avoid oligopoly. Furthermore, the fabrication of integrated devices such as OLEDs, storage batteries (supercapacitors), sensors, and solar cells would become much simpler by using multipurpose materials for different purposes at different layers of the integrated devices.

There are many mitigation strategies to improve the stability of perovskite solar cells, such as adding interconnecting materials such as polymers, defect management, humidity repulse additive incorporation, and adding excessive PbI_2. One of the reinforcement pathways is the control, reduction, or management of the number of grain boundaries, i.e., increasing the grain size, which is one technique to limit the repercussions of trap states and reduce hysteresis. Larger grains have a greater charge carrier mobility, an extended charge carrier lifetime, and a greater open-circuit voltage, all of which contribute to improved device efficiencies (Bai et al., 2017; Yuan et al., 2016). Furthermore, grain boundaries allow moisture to permeate through the perovskite films, resulting in deterioration (Rong et al., 2017). Applying such techniques as engineered doping, casting by temperature, and annealing by solvent, larger grains with uniform distribution can be formed, making perovskite films more resistant to moisture deterioration. Xu et al used $NH_4H_2PO_2$ (ammonium hypophosphite) as an additive to enhance grain size up to the μm range. Addition of additive, such as Phenyl-C61-butyric acid methyl ester (PCBM), could enhance the working of solar cells (Xu et al., 2018). In addition to PCBM, substituting iodide ions in MAPI with chloride ions decreases surplus iodine in the perovskite films, lowering trap state density and suppressing centers of recombination. Furthermore, several studies have used small organic molecules as a passivation layer to reduce non-radiative recombination sites and surface defects (Liu et al., 2018). Hence, mitigation and repurposing (like using OLED material in the solar cell) strategies are important tools to improve the viability of perovskite solar cell technology.

Conjugated polymers (CPs) are chemically inert, stable, and hydrophobic and can therefore protect perovskite SCs against humidity. CP has been extensively studied for its ability to produce ASE (amplified spontaneous emission) at different wavelengths of visible spectra (Aljaafreh et al., 2021a, Aljaafreh et al., 2021b), OLEDs (AlSalhi et al., 2011), and sensors (Li and Liu, 2010). Thiophene based CPs are specially made for solar cell applications but have occasionally also been used in laser applications (AlSalhi et al., 2018). The best polymer for solar cell applications is PEDOT: PSS due to its high electron conductivity (up to 1.8x10-3 sv/cm^{-3}). It is often used to replace the FTO and ITO layers in flexible solar cells; however, it has yet to or will never completely replace ITO and FTO without some performance compromises. At the same time, light-emitting CPs have also been utilized as hole conductive materials in perovskite solar cells. Masi et al fabricated a nanocomposite of CP MEH-PPV/$MAPbI_3$ perovskite that is dynamically used in solar cells. The polymer is utilized to control the inclusion of a small and uniform perovskite domain, leading to the fabrication of a smooth film using a single-step technique (Masi et al., 2015). Liren. Z et al. designed and synthesized various types of planar conjugated polymers that were primarily composed of bis(alkyloxy) benzene and/or bis(dithiophene) units. These polymeric materials act as hole transport layers in perovskite solar cells and can effectively act as a moisture barrier, preventing the perovskite from interacting directly with moisture (Zhang et al., 2019). The solid-state NMR (ss NMR) spectroscopy provides nanoscale insight into the blending nature of semi-ordered and amorphous regions; the remarkable insight provided by ssNMR about organic semiconductors and metal halide perovskites has been summarized by Seifrid et al. (2020), and Dahlman et al. (2021). Atomic-scale interaction between conjugated materials PM6 and Y6 in a bulk heterojunction (BHJ) and framework for understanding morphological differences and their impact on PCEs (Luginbuhl et al., 2022). The CP MDMO-PPV end-DMP produces laser at 560 nm and 605 nm (Prasad et al., 2020). It can be used to produce OLED and photoreactors. However, it is rarely used in solar cells and has not been used in combination with $MAPbI_{3-x}Cl_x$ as an active layer.

In this context, we report solar cells fabricated with red-emitting conjugated polymer MDMO-PPV as a hole transport layer, along with highly stable chlorine iodine mixed halide perovskite. The heterojunction solar cell (PEROVSKITE + CP)-based solar cell did not function well due to the low penetration of perovskite + CP into TiO_2 mesopores. When the thickness of the m-TiO_2 was adjusted to match the penetration of perovskite + CP, we were able to achieve better efficiency of our HJSC, and it remained stable for more than 4 weeks. To the best of our knowledge, this is the first report of a perovskite solar cell with the conjugated copolymer MDMO-PPV as a hole transport layer with a mesoporous TiO_2 architecture.

2. Materials and methods

The chemicals and solvents used in the experiment were acquired from commercial providers and used as received unless otherwise stated. Methylamine (33 wt%, absolute ethanol, titanium isopropoxide (TIP), hydroiodic acid (57 wt%, aqueous,), PbI_2, $PbCl_2$ were acquired from Sigma Aldrich, and diethyl ether VWR Chemicals, and were used in the preparation of methylammonium iodide (MAI). Fluoride-doped indium-doped tin oxide (FTO)-coated glass (15 O/cm^2) was purchased from Osilla, Sheffield, UK. The CP poly[2-methoxy-5-(3,7-dimethyloctyloxy)-1,4-phenylene-vinylene] (MDMO-PPV) was procured from an American dye source,. The crystal structure is typical of mixed halide perovskites, as depicted in Fig. 1a, and also illustrates the molecular structure of

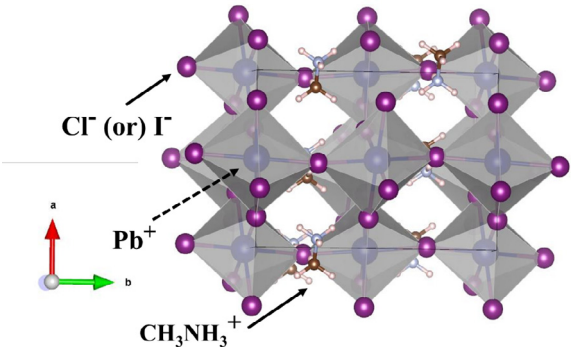

Fig. 1a. The crystal structure of unit drawing using VESTA software methylammonium mixed halide perovskite [35].

MDMO-PPV. TiO_2 nanoparticles were synthesized using a hydrothermal process reported earlier (Oh et al., 2009).

CPs have poor solubility in polar solvents. However, MDMO-PPV has two oxygens with 2 acceptor sites each; hence, it has good solubility in moderately polar solvents such as chlorobenzene (CB) and chloroform (CHF). We used CHF to dissolve MDMO-PPV. When the perovskite precursors in DMF and MDMO-PPV in CHF were mixed at 70 °C, they were completely miscible.

The absorption spectra were recorded using a PerkinElmer Lambda – 950, and the fluorescence spectra were obtained using a PerkinElmer LS 55. A nanosecond Ti:Sapphire laser was used for the ablation of FTO to provide isolation. We used Field Emission Scanning Electron Microscope (FE-SEM) was utilize to achieve high resolution images of SCs samples. The current voltage characteristics of the solar cells are performed using a FYTRONIX SM-9000 solar simulator and QE-9000 quantum efficiency system (Fig. 1(b)).

2.1. Computational studies of CP

The donor's LUMO and HOMO were determined to be −1.43 eV and −4.52 eV, respectively, as presented in Fig. 2(a). Fig. 2 (b) depicts the UV–VIS spectrum of MDMO-PPV (n = 3) calculated using the TD-DFT B3LYP method with a basis set of 6–31G*. The absorption spectrum exhibits a single prominent peak at a wavelength of 441.2 nm with an oscillator strength of 2.4; the oscillator strengths at 360 and 380 nm are insignificant, with oscillator strength values of 0.0038 and 0.0213, respectively. Nevertheless, experimental evidence indicates that these three oscillators are singlets and can be attributed to S0-0, S0-1, and S0-2. For n = 3, the donor's energy gap was approximately 3.09 eV. As illustrated in Fig. 2 (c), this CP exhibits a transition to a negative cotton effect from a positive cotton effect in its simulated ECD spectrum. This is

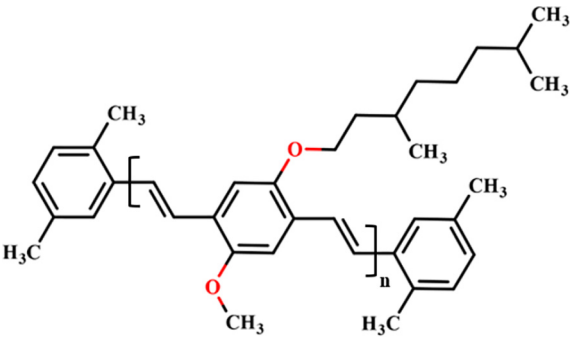

Fig. 1b. Molecular Structure of CP MDMO-PPV.

necessary for the MDMO-PPV to be polarizable. Fig. 2 (d) [inset of Fig 2b] shows the acceptor sites of CP.

Fig. 2(e) shows the estimated bandgap which is plotted against the inverse of repetitive monomer units, and the extrapolation up to n, which tends to infinity ($n \rightarrow \infty$) molecules. The intercept of the 1/n graph was 2.31 eV, which was compared to the experimental value of 2.25 eV as determined by the intersection of the absorption and fluorescence spectra method (yellow square). The calculated and experimental energy gaps differ by 0.06 eV, indicating that the simulated HOMO – LUMO structures and locus of the energy levels are extremely reliable. This is critical for comprehending the charge separation and interaction at the interface between the MDMO-PPV and perovskite.

2.2. Fabrication of solar cells

We kept the lab's relative humidity below 10 % using an air conditioner and dehumidifier. First, we etched a double line using laser ablation with a 355 nm, 5 ns pulsed laser. The isolation between the two area was more than 10 GΩ. Then, we cleaned the FTO substrate using sonication at 70 °C in deionized (DI) water with 1 % hellmanex and sonicated it for 30 min. We rinsed the substrate using boiling DI water and sonicated it for 30 min in acetone and absolute methanol. Again, it was rinsed in DI water and dried using lab air. Finally, we cleaned it under UV ozone for 10 min. As reported earlier, the compact and mesoporous layers were made using spin and doctors blade coating of TIP and synthesized TiO_2 nanoparticles (Prasad et al., 2018; Theerthagiri et al., 2017). The active layers (perovskite layer, MDMO-PPV, and mixed) were fabricated in an ambient atmosphere. We deposited $PbCl_2$ and PbI_2 (ratio 0.25:1.75) onto m-TiO_2 and then MAI onto m-TiO_2. Then, the samples were placed in a glass jar containing a silicon ball in a porous bag, and the air inside the jar was removed with a vacuum pump. Then, dry nitrogen was poured into the glass jar via another valve for 4 bar pressure. The high-pressure gas inside the jar was dehydrated (to similar humidity levels as those in the desert around Riyadh). This glass jar was placed on a hot plate at 100 °C for 60 min, the nitrogen was released to make 1 bar, and the samples were removed.

The hole transport layer (MDMP-PPV or LiTSO) was spin-coated at 2000 rpm. The gold layer was deposited by thermal evaporation. MDMO-PPV (20 mg/ml) was dissolved in chlorobenzene to spin-coat the hole transport layer. SpiroOMeTAD at a concentration of 97 mg/ml in chlorobenzene, Li-TFSI at a concentration of 175 mg/ml in acetonitrile, and TBP at a volumetric percentage of 46.6 percent in acetonitrile were dissolved to produce the hole transport layer. Then, we mixed 1000 µL of SpiroOMeTAD and 30.2 µL of Li-TFSI, after which 50 µL of the LiTSO solution was distributed onto the perovskite, allowing it to spread across the substrate and spin at 2000 rpm for 30 s to form the LiTSO layer.

3. Results and discussions

Optical absorption and photoluminescence emission spectroscopy on $MAPbI_{3-x}Cl_x$ were performed under ambient temperatures to understand the changes in the electronic structure of the mixed halide anion version with regard to the photon harvesting material, as depicted in Fig. 3. Fig. 3(a) represents the absorption spectra of a thin film perovskite with a thickness of 450 nm coated on a quartz substrate. The spectrum showed a bandgap transition at approximately 814 nm (1. 52 eV), which is typical of $MAPbI_{3-x}Cl_x$. It also showed a small dip at approximately 483 nm (2.57 eV). The $MAPbI_{3-x}Cl_x$ absorption band edge onset is centered at 760 nm at 24.85 °C, and we estimate the corresponding band gap to be 1.63 eV (using a bad edge method), which is consistent

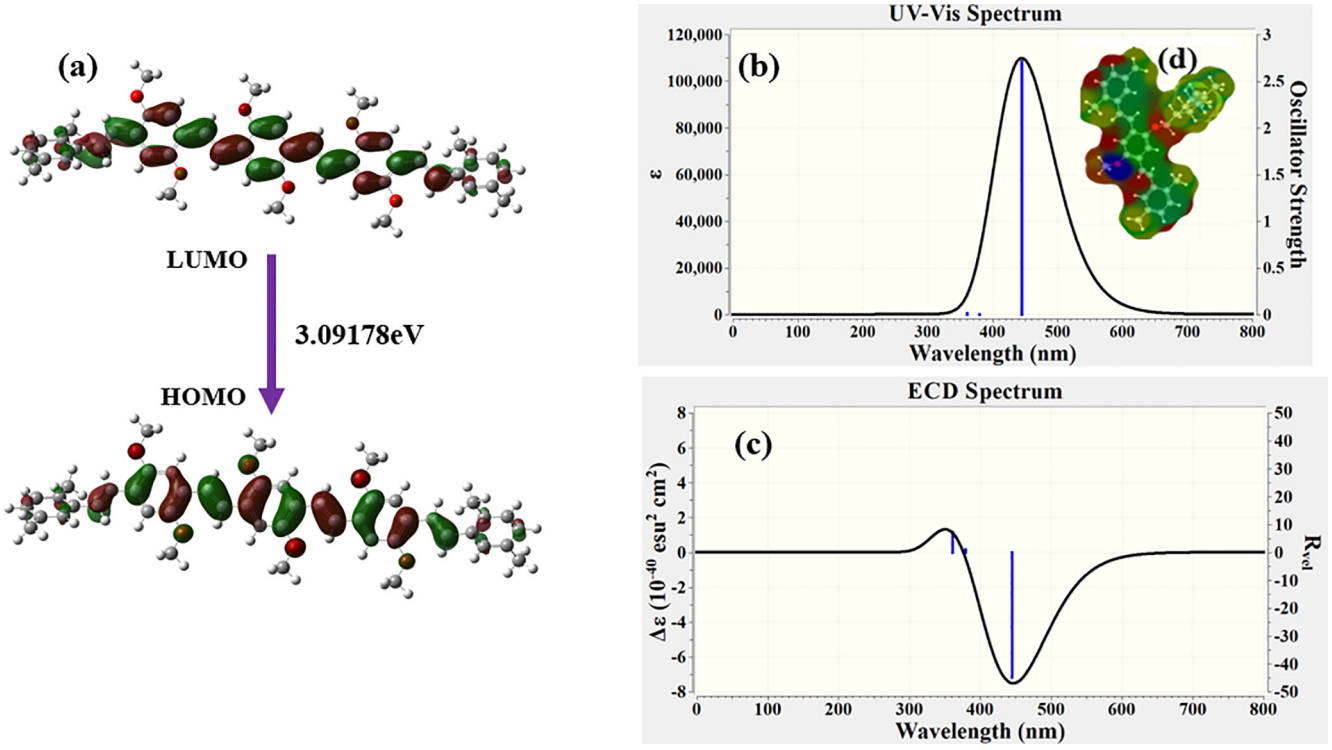

Fig. 2a. Simulated molecular orbitals structure (furrier densities), (2b) US-VIS and (2c) ECD structure of MDMO-PPV [n = 3] using TD-DFT B3LYP method with 6–31G basis set, and (2d) Acceptor sites of MDMO-PPV [inset of Fig 2b].

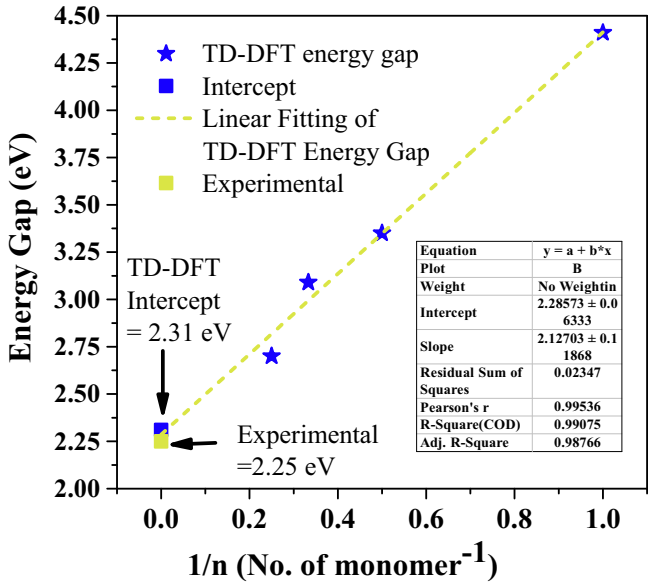

Fig. 2e. The estimated bandgap using oligomer model simulation up to n = 4 plotted against the inverse of repetitive monomer units, and extrapolation up to n tends to infinity (n → ∞) molecular and compared with experimentally estimated using the intersection of absorption and fluorescence spectra method (yellow square).

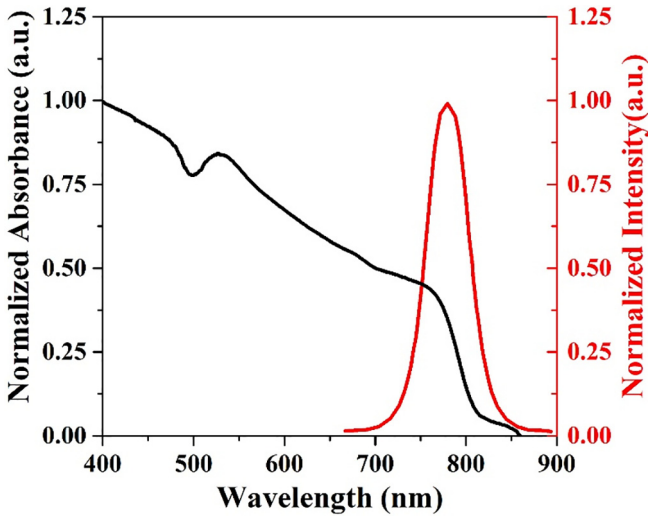

Fig. 3a. Normalized Absorption and fluorescence spectra of thin-film perovskite ($MAPbI_{3-x}Cl_x$) with a thickness of 450 nm coated on a quartz substrate.

with previous results (Zhang et al., 2016). The normalized fluorescence (red line) shows the peak at 781 nm and a large overlap between the absorption spectrum and has a Stokes shift of 20 nm.

The absorption spectrum of the MDMO-PPV absorption peak is approximately 488 nm for a thickness of 400 nm, which coincides with the dip in the absorption spectrum of $MAPbI_{3-x}Cl_x$, as presented in Fig. 3(b). The dip at 483 nm has been observed in many reports previously (Mehdi et al., 2020; Ralaiarisoa et al., 2019), and its origin could be attributed to grain boundary interface scattering and defect states. For typical nanomaterials, absorption increases towards shorter wavelengths. Similarly, the mix shows the perfect combination between MDMO-PPV and the $MAPbI_{3-x}Cl_x$ blend. The mix showed that absorption spectra of the blend are constructively superposed upon each other and add up to the sum of the individual components, indicating the nonappearance of strong interactions in the ground state.

The designed solar cells have both layered and heterojunction architectures. In general, the idea is to make a stable perovskite heterojunction layer that is resistant to environmental factors by

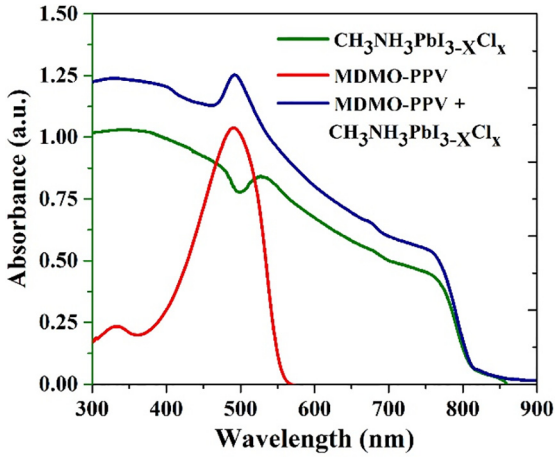

Fig. 3b. Absorption spectra of perovskite ($MAPbI_{3-x}Cl_x$), MDMO-PPV, and the blend of thin films of thickness 450 ± 30 nm coated on the quartz substrate.

using a conjugated polymer as both an encapsulation and hole transport material. One of the most significant prerequisites for optimum device performance in solar cells is an energy cascade enabled by the energy gradient between the light absorber, hole transport layer, and electron transport layer. The solar cell geometry consists of a homojunction or heterojunction layer of materials with energy levels given in a generalized energy diagram, as shown in Fig. 4. The energy levels of the various materials were taken from previously established reports (Heo and Im, 2016; Veenstra et al., 2004; Yuan et al., 2018; Zhang et al., 2018). The mixed perovskite has a valence band and conduction bands at −5.43 eV and −3.9 eV, respectively. The CO MDMO-PPV has HOMO and LUMO energies of −5.3 and −3, respectively. The large energy gradient between perovskite and MDMO-PPV largely stops the migration of electrons and enables charge separation at the interfacial junction. Additionally, LiTSO could be used as a bridge between HJ and Au. This is done because the mixing of perovskite and MDMO-PPV could reduce the bandgap and increase the barrier for the hole to jump from the perovskite/MDMO-PPV hybrid structure. We did not vary

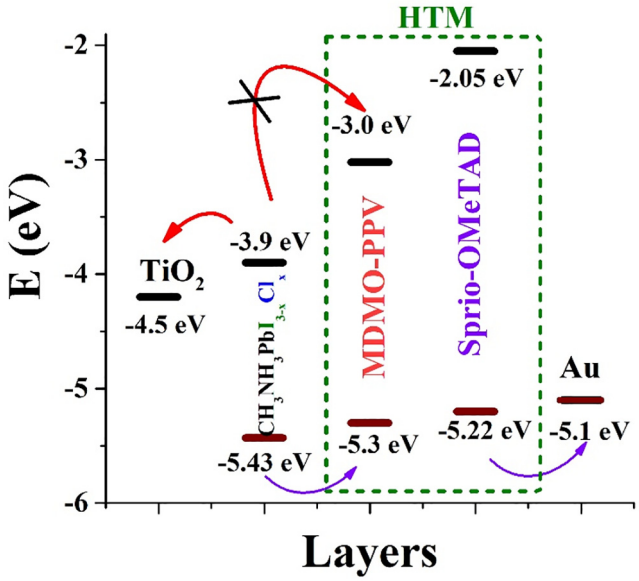

Fig. 4. Energy level of perovskite ($MAPbI_{3-x}Cl_x$), MDMO-PPV, and sprio-OMeTAD layers.

the thickness of MDMO-PPV, LiTSO, and gold (Au) to limit the permutation and combinations of the devices in this comparison study. The main objective was to compare the performance of devices fabricated under low humidity and easily achievable lab environments. The contact layer thickness was maintained at 85 ± 15 nm, and gold had an energy level of −4.5 eV.

The synthesized TiO_2 had high nanopore porosity, and the distribution showed that most of the particles were less than 100 nm in diameter, as shown in Fig. 5. The thickness of the m-TiO_2 layer varied from 400 nm to 800 nm. The inset of Fig. 5 shows the blend layer at the same magnification. The perovskite tends to form submicron and nanosized domains that are connected with MDMO-PPV polymers. The FESEM image also indicates that the blend film is smooth and continuous even at the very small region (nano level) or at the molecular level.

The device structure of a regular perovskite device Fig. 6 (a) (D1) contained the following layers: glass/FTO/m-TiO2/perovskite/LiTSO/Au. The perovskite layer was 460 nm and infiltrated into the m-TiO_2 layer. Apart from that, perovskite also formed a 100–90 nm thick layer on top of the perovskite layer LiTSO with a thickness of 120 nm and a contact layer of gold with a thickness of 80 nm. D1 showed a PCE of 7.68 % V_{oc} = 0.83, and J_{sc} was 14 mA. It is low compared to high-performance solar cells based on perovskite, but we have not employed sophisticated environmental conditions during fabrication. m-TiO_2-based perovskite solar cells are simple to fabricate; however, they are very sensitive to outside environments. The introduction of new processes, such as the addition of 1,8-diiodooctane (DIO), solvent vapor annealing (SVA) (Sun et al., 2016), and PANI, improves the performance of solar cells (Zheng et al., 2019). Similarly, the addition of CP could improve the stability of the SC, and hence, we employed CP MDMO-PPV.

The D2 device introduces MDMO-PPV as a hole conducting layer instead of LiTSO. The device of D2 is Glass/FTO/m-TiO2/perovskite/MDMO-PPV/Au, as shown in Fig. 6 (b). The performance is low again, with a PCE of 5.32 %, a V_{oc} of 0.836 V, with a lower open-circuit current J_{sc} of 13.25 mA and FF of 0.478. Fig. 6 (e) (D2) shows the solar cell structure and FESEM image. The TiO_2 layer was 415 ± 20 nm thick with a completely penetrated perovskite layer. The perovskite layer is topped with an MDMO-PPV layer with a thickness of 170 nm. D2 has good V_{oc} but a poor fill factor and thus performance; however, it has very high stability due to the presence of MDMO-PPV.

Next, we made HJSC with a blend layer (D3). The D3 was a set of solar cells will the same structure but with different thicknesses of the m-TiO_2. This type of devices has a structure with layers Glass/

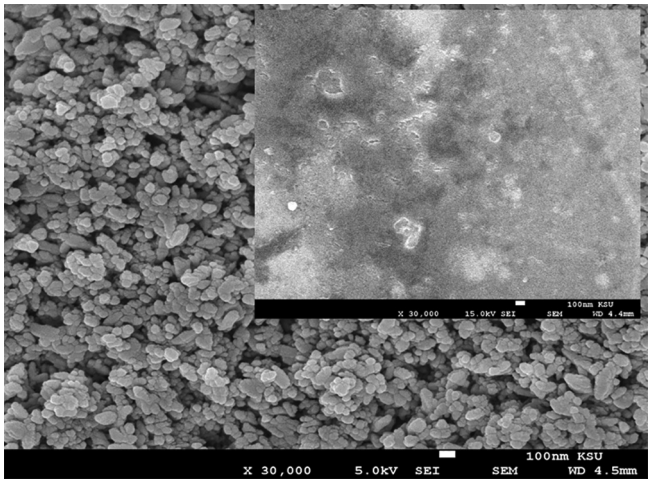

Fig. 5. FESEM image of TiO_2 and inset is the image of the blend.

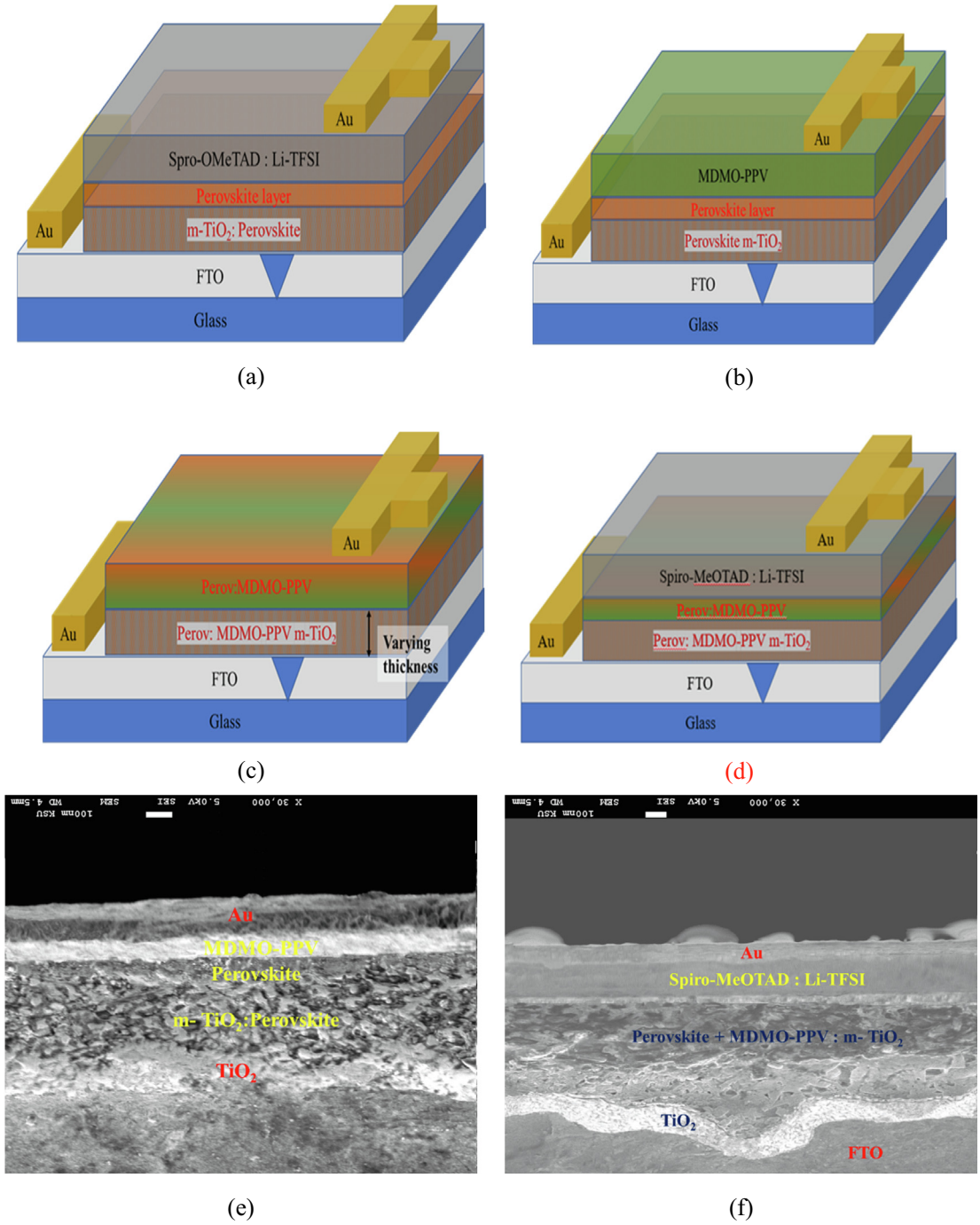

Fig. 6. (a-d) Device structure of solar cells and (e and f) FESEM of solar cells D2 and D3.

FTO/m-TiO_2/(Perovskite + MDMO-PPV)/Au, as shown in Fig. 6(c), which depicts one of the solar cells in D3 set. The penetration of blend inside m-TiO_2 was 250 ± 10 nm irrespective of the thickness of m-TiO_2, beyond m-TiO_2 thickness greater than 260 nm. The maximum efficiency was observed for m-TiO_2 thickness 300 nm. The thickness of the m-TiO_2 varied from 500 nm to 300 nm; the D3 devices have a PCE of 5.68 % to 7.43 % for higher and lower thicknesses, respectively. The FSEM image in Fig. 6(e) shows that the blended materials partially penetrated inside the m-TiO_2 by approximately 246 nm. The wide variation in PCE is obtained by changing the m-TiO_2 layer and by optimizing the thickness of MDMO-PPV. The reduction in the PCE could be attributed to two factors: (a) the perovskite + MDMO-PPV irregular contact made by the HJ and gold contact layer and (b) the blend not penetrating completely into m-TiO_2. The above issues could lead to increased recombination and lower charge separation. The other parameters of the HJSC (D3) type were a very low V_{oc} = 0.63–0.85 V, J_{sc} of 9.6 mA to 11.3 mA, and FF ranging from 0.5 to 0.68. The maximum efficiency in the D3 set of solar cells is given in the Fig. 7 (pink – star line), that with V_{oc} = 0.85 V, J_{sc} of 9.67 mA, FF of 0.68 and PCE of 7.438 %.

We aim to improve the efficiency of perovskite/MDMO-PPV solar cells using the following method. We first optimized the thickness of m-TiO_2 to 350 nm, and thus, the blended materials diffuse almost completely onto the m-TiO_2 layer. Thus, we introduce a layer of LiTSO with a PCE of 7.74 %, FF of 0.7 and V_{oc} = 0.89 V and J_{sc}

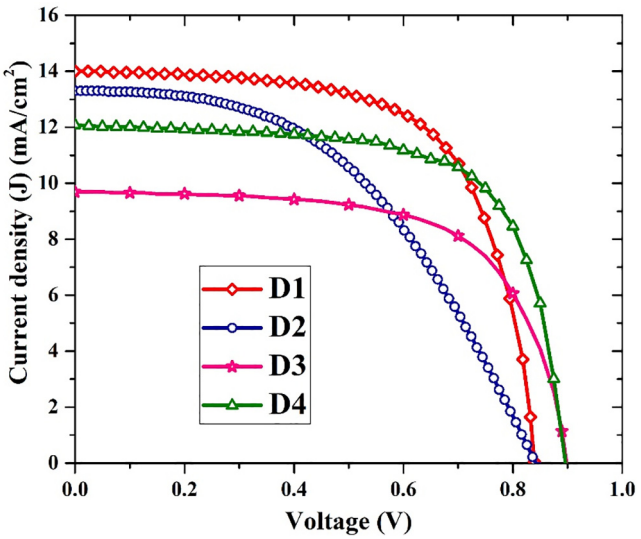

Fig. 7. The J–V characteristics for the solar cell's samples D1 – D4 types. (JV of D3 is maximum efficiency in the subset of D3 type solar cell).

of 12.07 mA (D4). The FSEM image shows a LiSTO base solar cell with layers of 78 ± 15 nm, 350 ± 10 nm, and 105 ± 15 nm of compact TiO_2, m-TiO_2 (MDMO-PPV/perovskite), and LiSTO, as shown in Fig. 6 (f).

Fig. 7 shows the JV curves of solar cell types D1, D2, and D4. The design of D3 involves a change in TiO_2 thickness. The depicted JV curve of D3 belongs to the maximum efficiency solar cell with an optimized thickness of m-TiO_2 (300 nm).

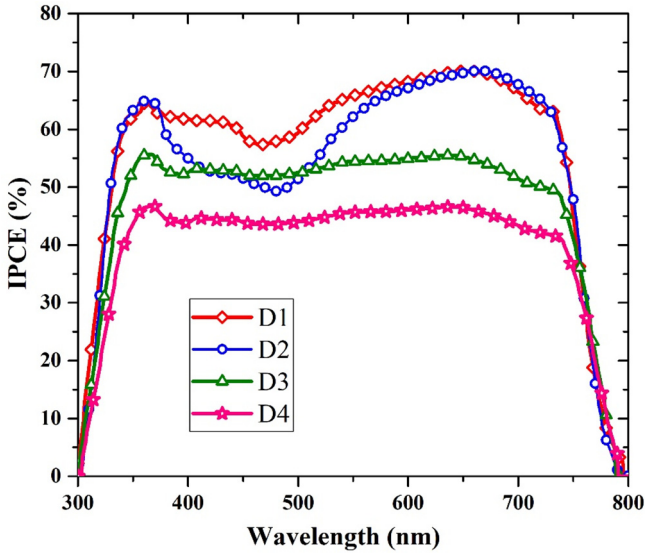

Fig. 8. IPCE spectra of the solar cells for all D samples.

The solar cells were randomly numbered and shuffled, and tested at another laboratory in a single-blind study. Additionally, the incident photon to charge carrier efficiency (IPCE) was measured at another laboratory. Fig. 8 shows the IPCE of devices D1 to D4. The J_{sc} calculated using IPCE was 13.89 mA for D1, 13.29 mA for D2, and 9.72 to 11.4 mA for D3 (group of different HJSC with different m-TiO_2 thicknesses), and for the last solar cell D4, the values were 11.52 mA.

To check the stability of the designed solar cells, the devices were connected to a 1 kΩ resistor as a load and exposed to sunlight and ambient atmosphere for a long time. The PEC of the solar cell was measured at weekly intervals. D1 dropped 22 % of its initial performance, D2 lost 13 %, and D3 showed 11 % lower performance after 4 weeks. The improved stability could be attributed to the molecular-level interaction between MDMO-PPV and perovskite. The plausible expiations are derived from the earlier insight provided by G. N. M. Reddy group (Krishna et al., 2021; Raval et al., 2022). The reduction in performance of D3-type solar cells with large m-TiO_2 could be due to the exposure of the microdomain of perovskite, and the uninfused m-TiO_2 layer could attract H_2O. Finally, the performance of D4-type HJSC with the LiSTO layer dropped by only 9 %. The solar cell devices of each type (D1 to D4) were fabricated and characterized at two different labs. The performance characteristics of different types of solar cells are tabulated in Table 1.

4. Conclusions

In this work, we designed a series of solar cells with mixed halide methylammonium perovskite active layers and a CP MDMO-PPV as an HTM in layered and heterojunction architecture. The layered solar cells (FTO/TiO_2/perovskite/MDMO-PPV/Au) have a high short circuit current density (J_{sc}) of 13.295 mA but a very poor fill factor (FF) of 0.47 and PCE of 5.32 %. The heterojunction solar cell (HJSC) made with perovskite, and MDMO-PPV mix showed a PCE of 5.68 % for the same thickness of m-TiO_2. The FESEM showed that in HJSC, the perovskite and CP were mixed well, but they did not penetrate deeply into the TiO_2 mesoporous layer, which hinders electron transportation and thus causes efficiency loss. Upon optimization of the thickness of m-TiO_2, the HJSC reached a PCE of 7.438 %. The added layer of LiTSO on top of the blend layer improved the PCE to 7.74 %, which is comparable to the performance of the standard perovskite solar cell fabricated under the same environmental and operational conditions. The usage of a conjugated polymer as a hole transport layer minimizes reliance on separate components while also increasing the stability of the solar cells. It could also pave the way for a simple, minimalistic solution for integrated, flexible power electronics that include perovskite/CP solar cells, an organic light-emitting diode, and a graphene supercapacitor.

CRediT authorship contribution statement

Saradh Prasad: Conceptualization, Methodology, Software, Validation, Formal analysis, Investigation, Data curation, Writing –

Table 1
The performance characteristics of different types of solar cells.

Device type	PCE (%)	V_{oc}	J_{sc}		FF
			JV	IPCE	
D1	7.68	0.83	14	13.89	0.66
D2	5.32	0.836	13.25	13.29	0.478
D3	5.684–7.438	0.88–0.89	9.6–11.3	9.72–11.4	0. 5–0.68
D4	7.74	0.89	12.50	12.02	0.70

original draft, Visualization. **Mamduh J. Aljaafreh:** Software, Validation, Formal analysis, Investigation, Data curation, Writing – original draft, Visualization. **Abeer Alshammari:** Formal analysis, Investigation, Visualization. **Mona A.S. Almutairi:** . **Jagannathan Madhavan:** Methodology, Writing – review & editing, Supervision. **Mohamad S. AlSalhi:** Conceptualization, Methodology, Validation, Resources, Writing – review & editing, Supervision, Project administration.

Declaration of Competing Interest

The authors declare that they have no known competing financial interests or personal relationships that could have appeared to influence the work reported in this paper.

Acknowledgements

This project was funded by the National Plan for Science, Technology, and Innovation (MAARIFAH), King Abdulaziz City for Science and Technology, Kingdom of Saudi Arabia, award number (14-ENE899-02).

Sample availability: available upon request

Samples of the fabricated samples are available from the corresponding author.

References

Aljaafreh, M.J., AlSalhi, M.S., Prasad, S., 2021a. Design of tunable liquid laser based on presence of the conjugated-polymer counter influencing the spectral properties of the oligomer. Opt. Mater. (Amst) 111, 110575.

Aljaafreh, M.J., Prasad, S., AlSalhi, M.S., Alhandel, R.H., Alsaigh, R.A., 2021b. TD-DFT Simulation and Experimental Studies of a Mirrorless Lasing of Poly [(9, 9-dioctylfluorenyl-2, 7-diyl)-co-(1, 4-diphenylene-vinylene-2-methoxy-5-{2-ethylhexyloxy}-benzene)]. Polymers (Basel). 13, 1430.

AlSalhi, M.S., Alam, J., Dass, L.A., Raja, M., 2011. Recent advances in conjugated polymers for light emitting devices. Int. J. Mol. Sci. 12, 2036–2054.

AlSalhi, M.S., Almotiri, A.R., Prasad, S., Aljaafreh, M.J., Othman, A.H.S., Masilamai, V., 2018. A temperature-tunable thiophene polymer laser. Polymers (Basel). 10, 470.

Bai, S., Sakai, N., Zhang, W., Wang, Z., Wang, J.-T.-W., Gao, F., Snaith, H.J., 2017. Reproducible planar heterojunction solar cells based on one-step solution-processed methylammonium lead halide perovskites. Chem. Mater. 29, 462–473.

Chen, Y., Peng, J., Su, D., Chen, X., Liang, Z., 2015. Efficient and balanced charge transport revealed in planar perovskite solar cells. ACS Appl. Mater. Interfaces 7, 4471–4475.

Dahlman, C.J., Kubicki, D.J., Reddy, G.N.M., 2021. Interfaces in metal halide perovskites probed by solid-state NMR spectroscopy. J. Mater. Chem. A 9, 19206–19244.

Heo, J.H., Im, S.H., 2016. Highly reproducible, efficient hysteresis-less CH 3 NH 3 PbI 3–x Cl x planar hybrid solar cells without requiring heat-treatment. Nanoscale 8, 2554–2560.

Huang, H., Shi, J., Zhu, L., Li, D., Luo, Y., Meng, Q., 2016. Two-step ultrasonic spray deposition of CH3NH3PbI3 for efficient and large-area perovskite solar cell. Nano Energy 27, 352–358.

Kim, H.-S., Lee, C.-R., Im, J.-H., Lee, K.-B., Moehl, T., Marchioro, A., Moon, S.-J., Humphry-Baker, R., Yum, J.-H., Moser, J.E., 2012. Lead iodide perovskite sensitized all-solid-state submicron thin film mesoscopic solar cell with efficiency exceeding 9%. Sci. Rep. 2, 1–7.

Kojima, A., Teshima, K., Shirai, Y., Miyasaka, T., 2009. Organometal halide perovskites as visible-light sensitizers for photovoltaic cells. J. Am. Chem. Soc. 131, 6050–6051.

Krishna, A., Zhang, H., Zhou, Z., Gallet, T., Dankl, M., Ouellette, O., Eickemeyer, F.T., Fu, F., Sanchez, S., Mensi, M., 2021. Nanoscale interfacial engineering enables highly stable and efficient perovskite photovoltaics. Energy Environ. Sci. 14, 5552–5562.

Leguy, A.M.A., Hu, Y., Campoy-Quiles, M., Alonso, M.I., Weber, O.J., Azarhoosh, P., Van Schilfgaarde, M., Weller, M.T., Bein, T., Nelson, J., 2015. Reversible hydration of CH3NH3PbI3 in films, single crystals, and solar cells. Chem. Mater. 27, 3397–3407.

Leijtens, T., Stranks, S.D., Eperon, G.E., Lindblad, R., Johansson, E.M.J., McPherson, I.J., Rensmo, H., Ball, J.M., Lee, M.M., Snaith, H.J., 2014. Electronic properties of meso-superstructured and planar organometal halide perovskite films: charge trapping, photodoping, and carrier mobility. ACS Nano 8, 7147–7155.

Li, K., Liu, B., 2010. Water-soluble conjugated polymers as the platform for protein sensors. Polym. Chem. 1, 252–259.

Liu, L., Huang, S., Lu, Y., Liu, P., Zhao, Y., Shi, C., Zhang, S., Wu, J., Zhong, H., Sui, M., 2018. Grain-Boundary "Patches" by In Situ Conversion to Enhance Perovskite Solar Cells Stability. Adv. Mater. 30, 1800544.

Luginbuhl, B.R., Raval, P., Pawlak, T., Du, Z., Wang, T., Kupgan, G., Schopp, N., Chae, S., Yoon, S., Yi, A., 2022. Resolving Atomic-Scale Interactions in Nonfullerene Acceptor Organic Solar Cells with Solid-State NMR Spectroscopy, Crystallographic Modelling, and Molecular Dynamics Simulations. Adv. Mater. 34. 2105943.

Masi, S., Colella, S., Listorti, A., Roiati, V., Liscio, A., Palermo, V., Rizzo, A., Gigli, G., 2015. Growing perovskite into polymers for easy-processable optoelectronic devices. Sci. Rep. 5, 1–7.

Mehdi, H., Matheron, M., Mhamdi, A., Manceau, M., Roux, C., Berson, S., Cros, S., Bouazizi, A., 2020. Correlation between efficiency and device characterization in MAPbI3-xClx standard perovskite solar cells. J. Mater. Sci. Mater. Electron. 31, 10251–10259.

Miyasaka, T., 2021. Perovskite Photovoltaics and Optoelectronics: From Fundamentals to Advanced Applications. John Wiley & Sons.

Noh, J.H., Im, S.H., Heo, J.H., Mandal, T.N., Seok, S.I., 2013. Chemical management for colorful, efficient, and stable inorganic–organic hybrid nanostructured solar cells. Nano Lett. 13, 1764–1769.

Oh, J.-K., Lee, J.-K., Kim, S.J., Park, K.-W., 2009. Synthesis of phase-and shape-controlled TiO2 nanoparticles via hydrothermal process. J. Ind. Eng. Chem. 15, 270–274.

Prasad, S., Durairaj, D., AlSalhi, M.S., Theerthagiri, J., Arunachalam, P., Durai, G., 2018. Fabrication of cost-effective dye-sensitized solar cells using sheet-like CoS2 films and phthaloylchitosan-based gel-polymer electrolyte. Energies 11, 281.

Prasad, S., Aljaafreh, M.J., AlSalhi, M.S., 2020. Time-resolved spectroscopy of radiative energy transfer between a conjugated oligomer and polymer in solution. Spectrochim. Acta Part A Mol. Biomol. Spectrosc. 232,. https://doi.org/10.1016/J.SAA.2020.118151 118151.

Qing, J., Chandran, H.-T., Cheng, Y.-H., Liu, X.-K., Li, H.-W., Tsang, S.-W., Lo, M.-F., Lee, C.-S., 2015. Chlorine incorporation for enhanced performance of planar perovskite solar cell based on lead acetate precursor. ACS Appl. Mater. Interfaces 7, 23110–23116.

Ralaiarisoa, M., Rodríguez, Y., Salzmann, I., Vaillant, L., Koch, N., 2019. Impact of solvent exposure on the structure and electronic properties of CH3NH3PbI3−xClx mixed halide perovskite films. Appl. Phys. A 125, 1–7.

Raval, P., Kennard, R.M., Vasileiadou, E.S., Dahlman, C.J., Spanopoulos, I., Chabinyc, M.L., Kanatzidis, M., Manjunatha Reddy, G.N., 2022. Understanding Instability in Formamidinium Lead Halide Perovskites: Kinetics of Transformative Reactions at Grain and Subgrain Boundaries. ACS Energy Lett. 7, 1534–1543.

Rong, Y., Hou, X., Hu, Y., Mei, A., Liu, L., Wang, P., Han, H., 2017. Synergy of ammonium chloride and moisture on perovskite crystallization for efficient printable mesoscopic solar cells. Nat. Commun. 8, 1–8.

Seifrid, M., Reddy, G.N., Chmelka, B.F., Bazan, G.C., 2020. Insight into the structures and dynamics of organic semiconductors through solid-state NMR spectroscopy. Nat. Rev. Mater. 5, 910–930.

Shao, Y., Xiao, Z., Bi, C., Yuan, Y., Huang, J., 2014. Origin and elimination of photocurrent hysteresis by fullerene passivation in CH3NH3PbI3 planar heterojunction solar cells. Nat. Commun. 5, 1–7.

Stranks, S.D., Eperon, G.E., Grancini, G., Menelaou, C., Alcocer, M.J.P., Leijtens, T., Herz, L.M., Petrozza, A., Snaith, H.J., 2013. Electron-hole diffusion lengths exceeding 1 micrometer in an organometal trihalide perovskite absorber. Science (80-.) 342, 341–344.

Sun, X., Zhang, C., Chang, J., Yang, H., Xi, H., Lu, G., Chen, D., Lin, Z., Lu, X., Zhang, J., 2016. Mixed-solvent-vapor annealing of perovskite for photovoltaic device efficiency enhancement. Nano Energy 28, 417–425.

Tan, W., Bowring, A.R., Meng, A.C., McGehee, M.D., McIntyre, P.C., 2018. Thermal stability of mixed cation metal halide perovskites in air. ACS Appl. Mater. Interfaces 10, 5485–5491.

Theerthagiri, J., Senthil, R.A., Arunachalam, P., Bhabu, K.A., Selvi, A., Madhavan, J., Murugan, K., Arof, A.K., 2017. Electrochemical deposition of carbon materials incorporated nickel sulfide composite as counter electrode for dye-sensitized solar cells. Ionics (Kiel). 23, 1017–1025.

Tvingstedt, K., Malinkiewicz, O., Baumann, A., Deibel, C., Snaith, H.J., Dyakonov, V., Bolink, H.J., 2014. Radiative efficiency of lead iodide based perovskite solar cells. Sci. Rep. 4, 1–7.

Veenstra, S.C., Verhees, W.J.H., Kroon, J.M., Koetse, M.M., Sweelssen, J., Bastiaansen, J., Schoo, H.F.M., Yang, X., Alexeev, A., Loos, J., 2004. Photovoltaic properties of a conjugated polymer blend of MDMO− PPV and PCNEPV. Chem. Mater. 16, 2503–2508.

Wehrenfennig, C., Eperon, G.E., Johnston, M.B., Snaith, H.J., Herz, L.M., 2014. High charge carrier mobilities and lifetimes in organolead trihalide perovskites. Adv. Mater. 26, 1584–1589.

Xu, W., Lei, G., Tao, C., Zhang, J., Liu, X., Xu, X., Lai, W., Gao, F., Huang, W., 2018. Precisely Controlling the grain sizes with an ammonium hypophosphite additive for high-performance perovskite solar cells. Adv. Funct. Mater. 28, 1802320.

Yang, Y., You, J., 2017. Make perovskite solar cells stable. Nature 544, 155–156.

Yuan, S., Wang, J., Yang, K., Wang, P., Zhang, X., Zhan, Y., Zheng, L., 2018. High efficiency MAPbI 3–x Cl x perovskite solar cell via interfacial passivation. Nanoscale 10, 18909–18914.

Yuan, Z., Yang, Y., Wu, Z., Bai, S., Xu, W., Song, T., Gao, X., Gao, F., Sun, B., 2016. Approximately 800-nm-thick pinhole-free perovskite films via facile solvent

retarding process for efficient planar solar cells. ACS Appl. Mater. Interfaces 8, 34446–34454.
Zhang, H., Liao, Q., Wang, X., Hu, K., Yao, J., Fu, H., 2016. Controlled substitution of chlorine for iodine in single-crystal nanofibers of mixed perovskite MAPbI3–xClx. Small 12, 3780–3787.
Zhang, W., Saliba, M., Moore, D.T., Pathak, S.K., Hörantner, M.T., Stergiopoulos, T., Stranks, S.D., Eperon, G.E., Alexander-Webber, J.A., Abate, A., 2015. Ultrasmooth organic–inorganic perovskite thin-film formation and crystallization for efficient planar heterojunction solar cells. Nat. Commun. 6, 1–10.
Zhang, L., Wu, J., Li, D., Li, W., Meng, Q., Bo, Z., 2019. Ladder-like conjugated polymers used as hole-transporting materials for high-efficiency perovskite solar cells. J. Mater. Chem. A 7, 14473–14477.
Zhang, P., Yang, F., Kapil, G., Shen, Q., Toyoda, T., Yoshino, K., Minemoto, T., Pandey, S.S., Ma, T., Hayase, S., 2018. Enhanced performance of ZnO based perovskite solar cells by Nb2O5 surface passivation. Org. Electron. 62, 615–620.
Zheng, H., Xu, X., Xu, S., Liu, G., Chen, S., Zhang, X., Chen, T., Pan, X., 2019. The multiple effects of polyaniline additive to improve the efficiency and stability of perovskite solar cells. J. Mater. Chem. C 7, 4441–4448.
Zheng, K., Zhu, Q., Abdellah, M., Messing, M.E., Zhang, W., Generalov, A., Niu, Y., Ribaud, L., Canton, S.E., Pullerits, T., 2015. Exciton binding energy and the nature of emissive states in organometal halide perovskites. J. Phys. Chem. Lett. 6, 2969–2975.